Reconstruction Formulas for Photoacoustic Sectional Imaging *

Peter Elbau[2], Otmar Scherzer[1,2] and Rainer Schulze[2]

[1]Computational Science Center
University of Vienna
Nordbergstr. 15
1090 Vienna, Austria

[2]Radon Institute of Computational
and Applied Mathematics
Altenberger Str. 69
4040 Linz, Austria

Abstract

The literature on reconstruction formulas for photoacoustic tomography (PAT) is vast. The various reconstruction formulas differ by used measurement devices and geometry on which the data are sampled. In standard photoacoustic imaging (PAI), the object under investigation is illuminated uniformly. Recently, sectional photoacoustic imaging techniques, using focusing techniques for initializing and measuring the pressure along a plane, appeared in the literature. This paper surveys existing and provides novel *exact* reconstruction formulas for sectional photoacoustic imaging.

1 Introduction

The literature on reconstruction formulas and back-projection algorithms for photoacoustic imaging is vast. Wang et al. developed reconstruction formulas for cylindrical, spherical, and planar measurement geometries in a series of papers [27, 25, 28], and recently many more algorithms based on reconstruction formulas have been developed (see the survey [13]).

Also different measurement devices for the ultrasound pressure have been suggested. Most common are small detectors based on materials, which exhibit a strong piezoelectric effect and can be immersed safely in water (i.e. polymers such as PVDF). In analytical reconstruction formulas, they are considered point detectors. Other experimental setups have been realized with line and area detectors, which collect averaged pressure (see [23] for a survey).

Here, we consider the problem of photoacoustic *sectional imaging*. As opposed to standard photoacoustic imaging, where the detectors record sets of two-dimensional projection images from which the three-dimensional imaging data can be reconstructed, *single slice imaging* reconstructs a set of two-dimensional slices, each by a single scan procedure. The advantages of the latter approach

---

are a considerable increase in measurement speed and the possibility to do selective plane imaging. In general, this can only be obtained by the cost of decreased out-of-plane resolution (i.e. the direction orthogonal to the focusing plane). Experimentally, one can obtain photoacoustic sectional imaging by illuminating a single plane of the object and by using a focused detector. Technical details are provided in Section 2. In our experiments, the measurement data are recorded on a cylindrical domain $\partial\Omega \times \mathbb{R}$, where $\partial\Omega$ denotes the boundary of a smooth domain Ω in $\mathbb{R}^2$.

The difference in this model to previously studied models is that the wave propagation is considered fully three-dimensional, the initialization *and* measurements are fully two-dimensional due to the selective plane illumination and detection. Therefore, such setups require novel reconstruction formulas. In particular, as a further novelty, we present reconstruction formulas in ellipsoidal domains.

This paper surveys existing and provides novel *exact* formulas for the reconstruction of the initial pressure distribution for various kinds of measurement setups. After the introduction of the *universal* back-projection algorithm introduced in [26] this goal seems superfluous, although not discussed in detail for sliced imaging. However, it has been shown recently by Natterer [17] that *universal* back-projection is only exact for special sampling geometries. Here, for sliced imaging and certain sampling setups, we can indeed find mathematically exact universal reconstruction algorithms for arbitrary strictly convex sampling domains Ω.

The paper is organized as follows: In Section 2, we describe the experimental setup of photoacoustic sectional imaging, and we model in Section 3 various measurements where it is possible to derive exact reconstructions formulas for sectional imaging. The reconstruction formulas are then provided in Section 4. In the appendix, we survey some background material on the Abel transform, the spherical mean operator, and the Mathieu equation.

2 Experimental Background

Below we give an overview on *photoacoustic sectional imaging*, describe the experimental realization, and provide mathematical formulations. In contrast, we call conventional photoacoustic imaging with uniform illumination of the object *non-focused*.

In general, PAI is based on the so called thermo- or photoacoustic effect. Laser light impinging onto a surface of an object leads to its heating and under the conditions of thermal and stress confinement an acoustic wave emerges from the object. Mathematically, this means that the initial pressure distribution p_0 is related to the absorption coefficient of the object by [3]

$$p_0(x) = \frac{\beta c^2}{C_p} \mu_a(x) \Phi(x) \tag{2.1}$$

where $x \in \mathbb{R}^3$. The constant prefactor consists of the thermal expansivity β, the specific heat capacity C_p and the speed of sound c. Then, μ_a is the absorption coefficient of the object and Φ denotes the local light fluency. Neglecting effects

of light propagation (i.e. setting Φ to be a constant), μ_a remains the only variable depending on x and containing the desired tomographic information about the object. Reconstruction algorithms that also take light propagation into account are investigated in Ref. [3] but are not focus of this work.

It is common to classify photoacoustic measurement setups into *point* (see e.g. [12]) and *integrating detector* setups [2]. The focus of this paper are reconstruction methods for sectional imaging and various kinds of detectors.

In conventional photoacoustic setups with point detectors, measurements are collected (see Fig. 1) all over a surface enclosing the object (i.e. a sphere or an ellipsoid), or all over a sufficiently large cylindrical surface (where the cross-section can be every line segment), or over a sufficiently large plane. The latter two detector array geometries allow for approximate reconstructions only, since sufficiently large means that in theory the array is considered infinitely large. This approximation causes the limited view problem in practical applications. Paltauf et al. have given correction factors for some of the affected geometries [22].
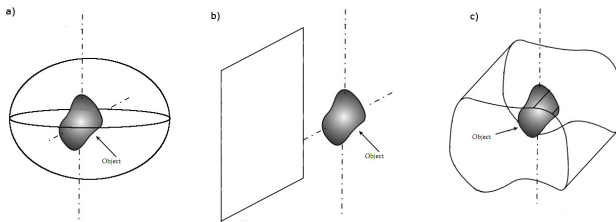

Figure 1: Sketch of non-focused point detector arrays. a) closed surface, b) quasi-infinite plane, c) cylindrical surface. The point detectors are spread over the indicated surfaces (points are not drawn in the figure). The detector arrays b) and c) suffer from the limited view problem.

The linear and planar detectors have to be moved tangentially to a surface surrounding the object (see [2]). Practically, this only allows the measurement devices to be aligned on a cylindrical surface (or on a plane). Experimental realizations of line detectors are documented for instance in [23].

In the following, we explain the principles of focusing detectors. The ultrasonic wave is refracted by a suitable acoustic lens such that out-of-plane signals are generally weak and can be neglected. Thus only signals emerging from the desired imaging plane are collected at the detector. Contemporary focusing ultrasonic detectors have a spherical or cylindrical shape, thus the detector surface plays the role of the acoustic lens. We consider the case of a cylindrically focusing detector, which focuses into a plane. The sectional imaging can be improved further by illuminating the desired plane only, i.e. by cylindrical lenses in front of the object. Note, however, that this requires a low scattering coefficient of the sample, because otherwise illumination will not be restricted to a single plane. The out-of-plane resolutions achieved are worse than the in-plane resolutions nevertheless. For more details on focusing point detectors see [15, 24] and for focusing line detectors see [7, 8].
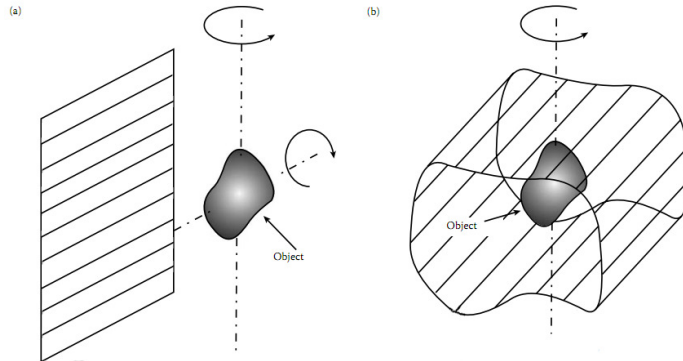
Figure 2: Sketch of non-focused line detector arrays. a) quasi-infinite plane, b) cylindrical surface with arbitrary cross-section. The detector array a) suffers from the limited view problem.

3   Mathematical Formulation

As an idealized model for the photoacoustic sectional imaging problem, we assume that the laser pulse which illuminates the sample is perfectly focused on the plane $\{x \in \mathbb{R}^3 \mid x_3 = 0\}$. We further consider the absorption of the laser light and the hereby caused expansion of the material to happen instanteneously, so that the induced initial pressure distribution $p_0 : \mathbb{R}^3 \to \mathbb{R}$ can be considered to be of the form

$$p_0(\xi, z) = \hat{p}_0(\xi)\delta(z), \quad \xi \in \mathbb{R}^2, \ z \in \mathbb{R}, \tag{3.1}$$

for some smooth function $\hat{p}_0 : \mathbb{R}^2 \to \mathbb{R}$ and with δ denoting the Dirac delta function. It will thus be often convenient for us to write a point $x \in \mathbb{R}^3$ in the form $x = (\xi, z)$ with $\xi \in \mathbb{R}^2$ and $z \in \mathbb{R}$.

This initial pressure distribution p_0 now initiates a pressure wave inside the object. Let $p(x; t)$ denote the pressure at the point $x \in \mathbb{R}^3$ at the time $t \in [0, \infty)$ after the laser pulse. For the propagation of the wave, we neglect the different material properties in the object and simply assume that the pressure distribution $p : \mathbb{R}^3 \times [0, \infty) \to \mathbb{R}$ obeys the linear three-dimensional wave equation with constant speed of sound, which we normalize to one:

$$\boxed{\begin{aligned} \partial_{tt}p(\xi, z; t) &= \Delta_{\xi, z}p(\xi, z; t), \\ \partial_t p(\xi, z; 0) &= 0, \\ p(\xi, z; 0) &= p_0(\xi, z) = \hat{p}_0(\xi)\delta(z) \end{aligned}} \tag{3.2}$$

for all $\xi \in \mathbb{R}^2$, $z \in \mathbb{R}$, and $t > 0$. Here, $\Delta_{\xi, z} = \partial_{\xi_1 \xi_1} + \partial_{\xi_2 \xi_2} + \partial_{zz}$ denotes the three-dimensional Laplacian in Euclidean coordinates.

Our aim is to recover the function $\hat{p}_0$, describing the initial pressure distribution, from certain measurements of the pressure wave p. From the initial pressure distribution, we may then determine the absorption coefficient μ_a of the object by using the relation (2.1), which is the final goal of the measurement.

4

The position of the detectors performing these measurements shall be given by the boundary $\partial\Omega$ of a convex domain $\Omega \subset \mathbb{R}^2$ in the illumination plane, where we additionally assume that $\hat{p}_0$ has compact support in Ω.

In practical realizations, the detectors usually have a special convex shape so that they mainly detect the pressure waves originating from the illumination plane and try to suppress those parts coming from an excitation outside this plane, as illustrated in Section 2. But since we assume a perfect focusing of the initial pressure distribution on the illumination plane in our model, we do not need this additional focusing by the detectors and will use simpler detector geometries. In a more realistic model, however, this suppression of signals from outside the illumination plane should be in some way incorporated into the mathematical model.

We will consider the following four different measurement setups and derive reconstruction formulas. Some of the reconstruction formulas and setups have already been documented in the literature and are surveyed here in the general context. Most of the formulas, however, are new.

Vertical Line Detectors: The measurement data are

$$m_1(\xi; t) := \int_{-\infty}^{\infty} p(\xi, z; t)\, dz$$
$$\text{for all } \xi \in \partial\Omega,\ t > 0. \tag{3.3}$$

That is, in practical realizations, we use *line detectors* which measure the overall pressure along a line orthogonal to the illumination plane.

Point Detectors: The measurement data are

$$m_2(\xi; t) := p(\xi, 0; t)$$
$$\text{for all } \xi \in \partial\Omega,\ t > 0. \tag{3.4}$$

That is, we use *point detectors* which measure the pressure on the boundary of $\partial\Omega$ over time. This measurement geometry is used in [15, 24].

For the other two measurement methods, we additionally impose that the domain $\Omega \subset \mathbb{R}^2$ is strictly convex and bounded.

Vertical Plane Detectors: The measurement data are

$$m_3(\theta; t) := \int_{P(\theta)} p(x; t)\, ds(x)$$
$$\text{for all } \theta \in S^1,\ t > 0, \tag{3.5}$$

where $P(\theta) \subset \mathbb{R}^3$ denotes the tangential plane of the cylinder $\partial\Omega \times \mathbb{R}$ orthogonal to the vector $(\theta, 0)$, see (3.8). For a practical realization we use *planar detectors* which are moved tangentially to $\partial\Omega$ around the object and measure the averaged pressure on the plane.

Horizontal Line Detectors: The measurement data are

$$m_4(\theta;t) := \int_{T(\theta)} p(\xi,0;t)\,ds(\xi)$$
$$\text{for all } \theta \in S^1,\ t > 0,$$

(3.6)

where $T(\theta) \subset \mathbb{R}^2$ denotes the tangential line of $\partial\Omega$ orthogonal to the vector θ, see (3.7). This is a realization using *line detectors* which measure the overall pressure on a line tangential to $\partial\Omega$ in the illumination plane, see [7, 8, 9]. (In these papers, they use for the reconstruction a phenomenologically motivated formula whose structure is very similar to the formula (4.13) which we derive for this sort of measurements.)

In those cases where the domain Ω is strictly convex and bounded, we parametrize the boundary $\partial\Omega$ with the map $\zeta : S^1 \to \partial\Omega$ which associates to every unit vector $\theta \in S^1$ the point $\zeta(\theta) \in \partial\Omega$ where the outward unit normal vector of $\partial\Omega$ coincides with θ, see Figure 3.
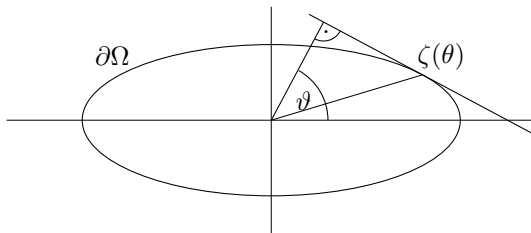

Figure 3: Definition of the point $\zeta(\theta)$, $\theta = (\cos\vartheta, \sin\vartheta)$.

Since the tangent line $T(\theta)$ of $\partial\Omega$ at $\zeta(\theta)$ is thus by definition orthogonal to θ, we can define the family $T(r,\theta)$, $r \in \mathbb{R}$, of lines parallel to the tangent $T(\theta)$ by

$$T(r,\theta) = \zeta(\theta) + r\theta + \mathbb{R}\theta^\perp \subset \mathbb{R}^2, \quad T(\theta) = T(0,\theta),$$

(3.7)

for every $\theta \in S^1$ and $r \in \mathbb{R}$. Here, $\theta^\perp \in S^1$ denotes a unit vector orthogonal to θ.

Moreover, we introduce the family $P(r,\theta)$, $r \in \mathbb{R}$, of planes parallel to the tangent plane $P(\theta)$ of the cylinder $\partial\Omega \times \mathbb{R}$ at $(\zeta(\theta),0)$ by

$$P(r,\theta) = (T(\theta),0) + (0,\mathbb{R}) \subset \mathbb{R}^3, \quad P(\theta) = P(0,\theta),$$

(3.8)

for every $\theta \in S^1$ and $r \in \mathbb{R}$.

4   Reconstruction Methods

In the following, we derive universal reconstruction formulas for photoacoustic sectional imaging. Conceptually, the paper is closely related to [14], where universal formulas for conventional photoacoustic tomography were derived in arbitrary geometry. However, some of the results there are implicit, requiring

explicit knowledge of eigenfunctions, which are provided here explicitly. Even more, the focus of this paper is on sectional imaging, which results in different formulas.

4.1 Measurements with Vertical Line Detectors

We introduce the function

$$\tilde{p}(\xi;t) = \int_{-\infty}^{\infty} p(\xi,z;t)\,dz, \quad \xi \in \mathbb{R}^2,\ t \geq 0. \tag{4.1}$$

Then the inital value problem (3.2) for the function p implies that the function $\tilde{p}$ satisfies the two-dimensional wave equation

$$\partial_{tt}\tilde{p}(\xi;t) = \Delta_\xi \tilde{p}(\xi;t) \quad \text{for all} \quad \xi \in \mathbb{R}^2,\ t > 0$$

with the initial conditions

$$\partial_t \tilde{p}(\xi;0) = 0 \qquad \text{for all} \quad \xi \in \mathbb{R}^2,$$
$$\tilde{p}(\xi;0) = \hat{p}_0(\xi) \quad \text{for all} \quad \xi \in \mathbb{R}^2.$$

The initially three-dimensional reconstruction problem therefore reduces to the two-dimensional problem of calculating $\hat{p}_0(\xi) = \tilde{p}(\xi;0)$, $\xi \in \mathbb{R}^2$, from the measurement data

$$m_1(\xi;t) = \tilde{p}(\xi;t), \quad \xi \in \partial\Omega,\ t > 0.$$

4.1.1 Reconstruction Formulas Based on Series Expansions

For special domains Ω, explicit reconstruction formulas are known: see the review [10] for Ω a circle and the half-space. The derivation for the ellipse is published in [4].

- If Ω is the half-space $\{\xi \in \mathbb{R}^2 \mid \xi_2 > 0\}$, we get [11]

$$\boxed{\hat{p}_0(\xi) = \frac{2}{\pi}\int_{-\infty}^{\infty}\int_k^{\infty}\tilde{m}_1(k,\omega)\mathrm{e}^{\mathrm{i}k\xi_1}\cos(\xi_2\sqrt{\omega^2-k^2})\,d\omega\,dk} \tag{4.2}$$

for every $\xi \in \mathbb{R}^2$, where

$$\tilde{m}_1(k,\omega) = \frac{1}{\pi}\int_{-\infty}^{\infty}\int_0^{\infty} m_1(\xi_1,0;t)\mathrm{e}^{-\mathrm{i}k\xi_1}\cos(\omega t)\,dt\,d\xi_1$$

is the Fourier–cosine transform of the measurement data m_1.

- If $\Omega = B_R^2(0)$ is the two-dimensional ball with radius R and center 0, we choose $\psi : [0,\infty) \times [0,2\pi) \to \mathbb{R}^2$, $\psi(r,\varphi) = (r\cos\varphi, r\sin\varphi)$, and get [10]

$$\boxed{\hat{p}_0(\psi(r,\varphi)) = \frac{1}{\pi}\int_0^{\infty}\sum_{k=-\infty}^{\infty}\frac{J_{|k|}(R\omega r)}{J_{|k|}(R\omega)}\tilde{m}_1(k,\omega)\mathrm{e}^{\mathrm{i}k\varphi}\,d\omega} \tag{4.3}$$

7

for every $r \in [0, \infty)$ and $\varphi \in [0, 2\pi)$, where

$$\tilde{m}_1(k, \omega) = \frac{1}{\pi} \int_0^\infty \int_0^{2\pi} m_1(\psi(R, \varphi); t) \mathrm{e}^{-\mathrm{i}k\varphi} \cos(\omega t) \, d\varphi \, dt$$

is the Fourier–cosine transform of the measurement data m_1. Here, J_k, $k \in \mathbb{N}_0$, denotes the kth Bessel function.

Equations (4.3) and (4.2) can be derived from formulas for the inversion of the spherical mean operator (see Section A.2), and this is why these formulas are typically assigned to Norton [18] and Norton & Linzer [19], although they considered reflectivity ultrasound imaging and here the topic is photoacoustics.

- If Ω is the ellipse $\{\xi \in \mathbb{R}^2 \mid \frac{\xi_1^2}{a^2} + \frac{\xi_2^2}{b^2} < 1\}$ with $a > b$, we set

$$\psi : [0, \infty) \times [0, 2\pi) \to \mathbb{R}^2, \quad \psi(r, \varphi) = \varepsilon \begin{pmatrix} \cosh(r) \cos(\varphi) \\ \sinh(r) \sin(\varphi)) \end{pmatrix},$$

with the linear eccentricity $\varepsilon = \sqrt{a^2 - b^2}$ and find [4]

$$\boxed{\hat{p}_0(\psi(r, \varphi)) = \frac{\sqrt{2}}{\pi} \int_0^\infty \sum_{k=0}^\infty \frac{R_k(r; \omega)}{R_k(r_0; \omega)} \tilde{m}_1(k, \omega) \Phi_k(\varphi; \omega) \, d\omega,}$$

where $r_0 = \mathrm{artanh}(\frac{b}{a})$ is chosen such that $\psi(r_0, \varphi) \in \partial\Omega$ and

$$\tilde{m}_1(k, \omega) = \frac{\sqrt{2}}{\pi} \int_0^\infty \int_0^{2\pi} m_1(\psi(r_0, \varphi); t) \Phi_k(\varphi; \omega) \cos(\omega t) \, d\varphi \, dt.$$

Herein, the functions Φ_k are for $k \in \mathbb{N}_0$ defined by

$$\Phi_{2k}(\varphi; \omega) = \mathrm{ce}_k(\varphi; \tfrac{\varepsilon^2 \omega^2}{4}) \quad \text{and} \quad \Phi_{2k+1}(\varphi; \omega) = \mathrm{se}_{k+1}(\varphi; \tfrac{\varepsilon^2 \omega^2}{4}),$$

where ce_k and se_k denote the Mathieu cosine and Mathieu sine functions, respectively, see Section A.4, and the functions R_k are the corresponding solutions of the radial Mathieu equation and are for $k \in \mathbb{N}_0$ given by

$$R_{2k}(r; \omega) = \mathrm{ce}_k(\mathrm{i}r; \tfrac{\varepsilon^2 \omega^2}{4}) \quad \text{and} \quad R_{2k+1}(r; \omega) = -\mathrm{i}\, \mathrm{se}_{k+1}(\mathrm{i}r; \tfrac{\varepsilon^2 \omega^2}{4}).$$

4.1.2 Reduction to the Spherical Mean Operator

Taking into account the relation (A.8) between the solution of the two-dimensional wave equation and the spherical mean operator, the problem of determining $\hat{p}_0$ from the measurements $m_1(\xi; t) = \tilde{p}(\xi; t)$ for $\xi \in \partial\Omega$, $t > 0$ can be equivalently described as the problem of reconstructing $\hat{p}_0$ from the spherical mean operator $\mathcal{M}_2[\hat{p}_0](\xi; r)$ of $\hat{p}_0$ for $\xi \in \partial\Omega$ and $r \in (0, \infty)$.

- For $\Omega = B_R^2(0) \subset \mathbb{R}^2$, analytical reconstruction formulas have been derived by Finch, Haltmeier, Rakesh [6] and read as follows

$$\boxed{\hat{p}_0(\xi) = \frac{1}{2\pi} \Delta_\xi \left(\int_{S^1} \int_0^{2R} r \mathcal{M}_2[\hat{p}_0](R\theta, r) \log|r^2 - |\xi - R\theta|^2| \, dr \, ds(\theta) \right)}$$

(4.4)

8

and

$$\hat{p}_0(\xi) = \frac{1}{2\pi} \int_{S^1} \int_0^{2R} \left(\partial_r r \partial_r \mathcal{M}_2[\hat{p}_0]\right)(R\theta, r) \log|r^2 - |\xi - R\theta|^2| \, dr \, ds(\theta).$$

(4.5)

- Recently, Palamodov derived in a more general setup analytical reconstruction formulas for some further special geometries. For Ω being e.g. the ellipse whose boundary is parametrized by the function $\psi : S^1 \to \mathbb{R}^2$, $\psi(\theta) = (a_1\theta_1, a_2\theta_2)$, $a_1, a_2 \in (0, \infty)$, he found the reconstruction formula

$$\hat{p}_0(\xi) = -\frac{4}{\int_{S^1} |\xi - \psi(\theta)|^{-2} \, ds(\theta)} \int_{S^1} \mathrm{P} \int_{-\infty}^{\infty} \frac{r^2 \mathcal{M}_2[\hat{p}_0](\psi(\theta), r^2)}{(|\xi - \psi(\theta)|^2 - r^2)^2} \, dr \, ds(\theta),$$

see [20, 21].

- For a general domain Ω, Kunyansky reduced in [14] the reconstruction problem to the determination of the eigenvalues λ_k and normalized eigenfunctions u_k, $\|u_k\|_2 = 1$, of the Dirichlet Laplacian $-\Delta$ on Ω with zero boundary conditions:

$$\Delta u_k(\xi) + \lambda_k u_k(\xi) = 0, \quad \xi \in \Omega, \tag{4.6}$$
$$u_k(\xi) = 0, \quad \xi \in \partial\Omega. \tag{4.7}$$

Indeed, if $(\xi, \eta) \mapsto G_{\lambda_k}(|\xi-\eta|)$ is a free-space rotationally invariant Green's function of the Helmholtz equation (4.6) and $n(\xi)$ denotes the outer unit normal vector of $\partial\Omega$ at $\xi \in \partial\Omega$, then

$$\hat{p}_0(\xi) = 2\pi \sum_{k=0}^{\infty} \tilde{M}_k u_k(\xi), \tag{4.8}$$

where

$$\tilde{M}_k = \int_{\partial\Omega} \int_0^{\infty} r \mathcal{M}_2[\hat{p}_0](\eta, r) G_{\lambda_k}(r) \langle \nabla u_k(\eta), n(\eta) \rangle \, dr \, ds(\eta).$$

We thus get the initial pressure distribution $\hat{p}_0$ by first calculating from the measurements $m_1(\xi; t) = \tilde{p}(\xi; t)$, $\xi \in \partial\Omega$, $t > 0$, with formula (A.8) the spherical mean operator $\mathcal{M}_2[\hat{p}_0](\xi; r)$ of $\hat{p}_0$ for $\xi \in \partial\Omega$ and $r \in (0, \infty)$, and then using one of the formulas (4.4), (4.5), or (4.8) to get $\hat{p}_0$.

4.2 Measurements with Point Detectors

From equation (A.7), we know that the solution of the initial value problem (3.2) can be for every $x \in \mathbb{R}^3$ and $t > 0$ written in the form

$$p(x; t) = \partial_t \left(\frac{1}{4\pi t} \int_{\partial B_t^3(0)} f(x + y) \, ds(y) \right).$$

9

Parameterizing the sphere $\partial B_t^3(0)$ in cylindrical coordinates, i.e. in the form

$$\partial B_t^3(0) = \left\{ (\sqrt{t^2 - h^2}\,\theta, h) \; : \; h \in [-t, t],\; \theta \in S^1 \right\},$$

we find for every $x = (\xi, z)$, $\xi \in \mathbb{R}^2$, $z \in \mathbb{R}$, and $t > 0$ that

$$p(\xi, z; t) = \partial_t \left(\frac{1}{4\pi t} \int_{-t}^t \int_{S^1} \hat{p}_0(\xi + \sqrt{t^2 - h^2}\,\theta)\delta(z + h)t\,ds(\theta)\,dh \right),$$

where we have used the special property of the source term (3.1). Integrating out the δ-distribution, we get for $z \in [-t, t]$

$$p(\xi, z; t) = \partial_t \left(\frac{1}{4\pi} \int_{S^1} \hat{p}_0(\xi + \sqrt{t^2 - z^2}\,\theta)\,ds(\theta) \right). \tag{4.9}$$

By the definition (A.4) of the spherical mean operator $\mathcal{M}_2$, this means

$$p(\xi, z; t) = \frac{1}{2}\partial_t\big(\mathcal{M}_2[\hat{p}_0](\xi; \sqrt{t^2 - z^2})\big) \quad \text{for} \quad z \in [-t, t]. \tag{4.10}$$

From the assumption that the support of $\hat{p}_0$ lies completely in Ω, we know that $\mathcal{M}_2[\hat{p}_0](\xi; 0) = \hat{p}_0(\xi) = 0$ for $\xi \notin \Omega$. Thus, we can integrate the relation (4.10) for $\xi \notin \Omega$ and find for every $z \in [-t, t]$ that

$$\mathcal{M}_2[\hat{p}_0](\xi; \sqrt{t^2 - z^2}) = 2 \int_z^t p(\xi, z; \tilde{t})\,d\tilde{t}.$$

Setting $z = 0$, we get for every $\xi \in \partial\Omega$ and every $t > 0$ the relation

$$\boxed{\mathcal{M}_2[\hat{p}_0](\xi; t) = 2 \int_0^t m_2(\xi; \tilde{t})\,d\tilde{t}.}$$

Having calculated the spherical mean of $\hat{p}_0$, we can now proceed as in Section 4.1.2.

4.3 Measurements with Vertical Plane Detectors

For every $\theta \in S^1$, we define for $r \in \mathbb{R}$ and $t \geq 0$ the function

$$\tilde{p}_\theta(r; t) = \int_{P(r,\theta)} p(x; t)\,ds(x),$$

where $P(r, \theta)$ denotes the plane as defined in (3.8).

Then, since the vectors $(\theta, 0)$, $(\theta^\perp, 0)$, and $(0, 0, 1)$ form an orthonormal basis of $\mathbb{R}^3$ and the Laplacian is rotationally invariant, we find from equation (3.2) that

$$\partial_{tt}\tilde{p}_\theta(r; t) = \int_{-\infty}^\infty \int_{-\infty}^\infty \Delta_x p(\zeta(\theta) + r\theta + u\theta^\perp, z; t)\,du\,dz = \partial_{rr}\tilde{p}_\theta(r; t)$$

for every $r \in \mathbb{R}$ and $t > 0$. Thus, $\tilde{p}_\theta$ solves the one-dimensional wave equation with the initial conditions

$$\begin{aligned}
\partial_t \tilde{p}_\theta(r; 0) &= 0 && \text{for all } r \in \mathbb{R} \text{ and} \\
\tilde{p}_\theta(0; t) &= m_3(\theta; t) && \text{for all } t > 0
\end{aligned}$$

10

resulting from (3.2) and (3.5), respectively. Moreover, since $\hat{p}_0$ has its support inside Ω, we know that $\tilde{p}_\theta(r; 0) = 0$ for $r \geq 0$.

With d'Alembert's formula for the solution of the one-dimensional wave equation, we find that the unique solution for this initial value problem is given by

$$\tilde{p}_\theta(r; t) = m_3(\theta; -t - r) + m_3(\theta; t - r), \quad r \in \mathbb{R}, \ t > 0,$$

where we set $m_3(\theta; t) = 0$ for $t \leq 0$.

Finally, we have to recover from the values of $\tilde{p}_\theta$, $\theta \in S^1$, the initial pressure distribution p_0 from equation (3.2). We have the relation

$$\tilde{p}_\theta(r; 0) = \int_{-\infty}^\infty \hat{p}_0(\zeta(\theta) + r\theta + u\theta^\perp) \, du = \mathcal{R}[\hat{p}_0](r + \langle \zeta(\theta), \theta \rangle, \theta),$$

where $\mathcal{R}$ denotes the Radon transform as defined in (A.9). We can therefore recover $\hat{p}_0$ with an inverse Radon transform:

$$\boxed{\hat{p}_0 = 2\mathcal{R}^{-1}[\tilde{m}_3], \quad \tilde{m}_3(r, \theta) = \begin{cases} m_3(\theta; \langle \zeta(\theta), \theta \rangle - r) & \text{if } r < \langle \zeta(\theta), \theta \rangle, \\ 0 & \text{if } r \geq \langle \zeta(\theta), \theta \rangle. \end{cases}} \quad (4.11)$$

Equation (4.11) reveals an interesting property of integrating area detectors: For an arbitrary strictly convex measurement geometry Ω, exact reconstruction formulas exist. This is a property which is not known for conventional and other photoacoustic sectional imaging technologies.

4.4 Measurements with Horizontal Line Detectors

For every $\theta \in S^1$, we define the function

$$\tilde{p}_\theta(r, z; t) = \int_{T(r, \theta)} p(\xi, z; t) \, ds(\xi),$$

where $T(r, \theta)$ is defined as in (3.7). Then, using that the vectors $(\theta, 0)$, $(\theta^\perp, 0)$, and $(0, 0, 1)$ are an orthonormal basis of $\mathbb{R}^3$ and that the Laplacian is rotationally invariant, the initial value problem (3.2) implies that $\tilde{p}_\theta$ solves for all $r, z \in \mathbb{R}$ and $t > 0$ the two-dimensional wave equation

$$\partial_{tt}\tilde{p}_\theta(r, z; t) = \int_{-\infty}^\infty \Delta_x p(\zeta(\theta) + r\theta + u\theta^\perp, z; t) \, du$$
$$= \partial_{rr}\tilde{p}_\theta(r, z; t) + \partial_{zz}\tilde{p}_\theta(r, z; t)$$

with the initial conditions

$$\partial_t \tilde{p}_\theta(r, z; 0) = 0,$$
$$\tilde{p}_\theta(r, z; 0) = P_\theta(r)\delta(z), \quad P_\theta(r) = \int_{T(r, \theta)} \hat{p}_0(\xi) \, ds(\xi),$$

for every $r, z \in \mathbb{R}$.

From formula (A.6), we see that the solution of this initial value problem can be written as

$$\tilde{p}_\theta(r,z;t) = \frac{1}{2\pi}\partial_t\left(\int_{B_t^2(0)} \frac{P_\theta(r+\rho)\delta(z+\zeta)}{\sqrt{t^2-\rho^2-\zeta^2}}\, ds(\rho,\zeta)\right)$$

$$= \frac{1}{2\pi}\partial_t\left(\int_{-t}^{t}\delta(z+\zeta)\int_{-\sqrt{t^2-\zeta^2}}^{\sqrt{t^2-\zeta^2}} \frac{P_\theta(r+\rho)}{\sqrt{t^2-\rho^2-\zeta^2}}\, d\rho\, d\zeta\right)$$

for all $r,z \in \mathbb{R}$ and $t > 0$. Integrating out the δ-function, we find for every $z \in [-t,t]$ that

$$\tilde{p}_\theta(r,z;t) = \frac{1}{2\pi}\partial_t\left(\int_{-\sqrt{t^2-z^2}}^{\sqrt{t^2-z^2}} \frac{P_\theta(r+\rho)}{\sqrt{t^2-z^2-\rho^2}}\, d\rho\right).$$

Since $\tilde{p}_\theta$ is related to the measurement m_4, given by (3.6), via $m_4(\theta;t) = \tilde{p}_\theta(0,0;t)$, and since $P_\theta(r) = 0$ for $r > 0$ by the assumption that $\hat{p}_0$ has support inside Ω, we find with the formula (A.1) for the Abel transform in reciprocal coordinates that

$$m_4(\theta;t) = \frac{1}{2\pi}\partial_t\left(\int_0^t \frac{P_\theta(-\rho)}{\sqrt{t^2-\rho^2}}\, d\rho\right) = \frac{1}{4\pi}\partial_t\left(\tfrac{1}{t}\mathcal{A}[\psi_\theta](\tfrac{1}{t})\right)$$

where $\psi_\theta(\frac{1}{\rho}) = \rho^2 P_\theta(-\rho)$. Switching to the reciprocal coordinate $s = \frac{1}{t}$ and using the identity (A.3), we see that this is of the form

$$\frac{2}{s^2}m(\theta;\tfrac{1}{s}) = -\frac{1}{2\pi}\partial_s\big(s\mathcal{A}[\psi_\theta](s)\big) = \mathcal{A}^{-1}[\tilde{\psi}_\theta](s)$$

with $\tilde{\psi}_\theta(\frac{1}{\rho}) = \frac{1}{\rho^2}\psi_\theta(\frac{1}{\rho}) = P_\theta(-\rho)$. Thus, we can directly solve the equation for P_θ and find

$$P_\theta(-\rho) = 2\mathcal{A}[\tilde{m}_\theta](\tfrac{1}{\rho}), \quad \tilde{m}_\theta(\tfrac{1}{t}) = t^2 m_4(\theta;t). \tag{4.12}$$

Since we have by definition

$$P_\theta(r) = \mathcal{R}[\hat{p}_0](r + \langle\zeta(\theta),\theta\rangle, \theta),$$

we finally get (remembering that $P_\theta(r) = 0$ for $r \geq 0$)

$$\boxed{\hat{p}_0 = 2\mathcal{R}^{-1}[\tilde{P}], \quad \tilde{P}(r,\theta) = \begin{cases} \mathcal{A}[\tilde{m}_\theta]\left(\frac{1}{\langle\zeta(\theta),\theta\rangle-r}\right) & \text{if } r < \langle\zeta(\theta),\theta\rangle, \\ 0 & \text{if } r \geq \langle\zeta(\theta),\theta\rangle. \end{cases}} \tag{4.13}$$

So, the reconstruction of $\hat{p}_0$ can be accomplished by an Abel transform of the rescaled measurements $\tilde{m}_\theta$, defined in (4.12), followed by an inverse Radon transform. Again, this reconstruction formula is valid for an arbitrary strictly convex measurement geometry Ω.

Conclusion

In this paper we have surveyed exact reconstruction formulas for photoacoustic sectional imaging. All formulas are mathematically, analytically exact. Comparing point and integrating line detectors, it is quite surprising that integrating area detectors allow analytical reconstructions for all strictly convex domains. This property has not been observed for point detectors.

A   Appendix

A.1   Abel Transform

The *Abel transform* $\mathcal{A}[\psi]$ of a smooth function $\psi : \mathbb{R}_+ \to \mathbb{R}$, which decays sufficiently fast to zero at ∞, is defined by

$$\mathcal{A}[\psi](y) = \int_{-\infty}^{\infty} \psi(\sqrt{x^2 + y^2})\, dx = 2 \int_y^{\infty} \frac{r\psi(r)}{\sqrt{r^2 - y^2}}\, dr, \quad y \geq 0.$$

We rewrite the Abel transform in reciprocal coordinates, so that it better fits in our context. Substituting $y = \frac{1}{t}$ and $r = \frac{1}{s}$, we find that

$$\mathcal{A}[\psi](\tfrac{1}{t}) = 2 \int_{\frac{1}{t}}^{\infty} \frac{tr\psi(r)}{\sqrt{r^2 t^2 - 1}}\, dr = 2 \int_0^t \frac{t\psi(\frac{1}{s})}{s^2 \sqrt{t^2 - s^2}}\, ds. \tag{A.1}$$

To invert the Abel transform, we remark that we have for all $v \geq 0$

$$\int_{-\infty}^{\infty} \frac{(\mathcal{A}[\psi])'(\sqrt{u^2 + v^2})}{\sqrt{u^2 + v^2}}\, du = \int_{-\infty}^{\infty} \int_{-\infty}^{\infty} \frac{\psi'(\sqrt{x^2 + u^2 + v^2})}{\sqrt{x^2 + u^2 + v^2}}\, du\, dx$$

$$= 2\pi \int_v^{\infty} \psi'(\rho)\, d\rho = -2\pi \psi(v),$$

where we substituted $x = \sqrt{\rho^2 - v^2} \cos(\varphi)$ and $u = \sqrt{\rho^2 - v^2} \sin(\varphi)$. Therefore, the *inverse Abel transform* $\mathcal{A}^{-1}[\psi]$ of a function $\psi : \mathbb{R}_+ \to \mathbb{R}$ can be written as

$$\mathcal{A}^{-1}[\psi](y) = -\frac{1}{2\pi y}(\mathcal{A}[\psi])'(y). \tag{A.2}$$

Using the identity

$$(\mathcal{A}[r^2 \psi])'(y) = \partial_y \left(\int_{-\infty}^{\infty} (x^2 + y^2)\psi(\sqrt{x^2 + y^2})\, dx \right)$$

$$= \partial_y \left(y^2 \mathcal{A}[\psi](y) \right) + \int_{-\infty}^{\infty} \frac{x^2 y}{\sqrt{x^2 + y^2}} \psi'(\sqrt{x^2 + y^2})\, dx$$

$$= \partial_y \left(y^2 \mathcal{A}[\psi](y) \right) - y \int_{-\infty}^{\infty} \psi(\sqrt{x^2 + y^2})\, dx = y \partial_y \left(y\mathcal{A}[\psi](y) \right),$$

and using (A.2) we can also write the inverse Abel transform in the form

$$\mathcal{A}^{-1}[r^2 \psi](y) = -\frac{1}{2\pi} \partial_y \left(y\mathcal{A}[\psi](y) \right). \tag{A.3}$$

A.2   Circular and Spherical Means

Let $x \in \mathbb{R}^n$ and $r \geq 0$. The *spherical mean operator* in $\mathbb{R}^n$ of an integrable function $f : \mathbb{R}^n \to \mathbb{R}$ is defined by

$$\mathcal{M}_n[f](x; r) = \frac{1}{|S^{n-1}|} \int_{S^{n-1}} f(x + r\theta)\, ds(\theta), \tag{A.4}$$

where $|S^{n-1}|$ denotes the area of the unit sphere S^{n-1} in $\mathbb{R}^n$.

The spherical mean value operator is closely related to the solution of the n-dimensional wave equation

$$\partial_{tt} p(x;t) = \Delta_x p(x;t),$$
$$\partial_t p(x;0) = 0,$$
$$p(x;0) = f(x)$$

for all $x \in \mathbb{R}^n$ and $t > 0$. More precisely, the solution p can be expressed in terms of the spherical mean operator of f by (see e.g. [5])

$$p(x;t) = \frac{1}{(n-2)!} \partial_t^{n-1} \left(\int_0^t r(t^2 - r^2)^{(n-3)/2} \mathcal{M}_n[f](x;r) \, dr \right)$$

for all $x \in \mathbb{R}^n$ and $t > 0$. In particular, we have for

- $n = 2$ that the solution p of the two-dimensional wave equation can be calculated from the spherical means via the Abel transform (A.1):

$$p(x;t) = \partial_t \left(\int_0^t \frac{r \mathcal{M}_2[f](x;r)}{\sqrt{t^2 - r^2}} \, dr \right) = \partial_t \left(\frac{1}{2t} \mathcal{A}[\tilde{f}_x](\tfrac{1}{t}) \right), \qquad (\text{A.5})$$

  where $\tilde{f}_x(\tfrac{1}{r}) := r^3 \mathcal{M}_2[f](x,r)$, leading also to the formula

$$p(x;t) = \frac{1}{2\pi} \partial_t \left(\int_{B_t^2(0)} \frac{f(x+y)}{\sqrt{t^2 - |y|^2}} \, ds(y) \right) \qquad (\text{A.6})$$

  for all $x \in \mathbb{R}^2$, $t > 0$, where $B_t^2(0) \subset \mathbb{R}^2$ denotes the two-dimensional ball with radius t and center 0;

- and for $n = 3$, we get that the solution p of the three-dimensional wave equation and $\mathcal{M}_3[f]$ are related by

$$p(x;t) = \partial_t \big(t \mathcal{M}_3[f](x;t) \big) = \partial_t \left(\frac{1}{4\pi t} \int_{\partial B_t^3(0)} f(x+y) \, ds(y) \right) \qquad (\text{A.7})$$

  for all $x \in \mathbb{R}^3$, $t > 0$, where $\partial B_t^3(0)$ denotes the boundary of the three-dimensional ball $B_t^3(0) \subset \mathbb{R}^3$ with radius t and center 0.

We remark that we can solve the equations (A.5) and (A.7) for the spherical mean operator of f. We get for $n = 2$ with $s = \frac{1}{t}$ that

$$\frac{1}{\pi s^2} p(x; \tfrac{1}{s}) = -\frac{1}{2\pi} \partial_s \big(s \mathcal{A}[\tilde{f}_x](s) \big),$$

which gives us with the representation (A.3) of the inverse Abel transform that

$$\mathcal{M}_2[f](x;r) = \frac{1}{\pi r} \mathcal{A}[\tilde{p}_x](\tfrac{1}{r}) = \frac{2}{\pi} \int_0^r \frac{p(x,t)}{\sqrt{r^2 - t^2}} \, dt, \quad x \in \mathbb{R}^2, \ r > 0, \qquad (\text{A.8})$$

where $\tilde{p}_x(\tfrac{1}{t}) = t^2 p(x;t)$; and for $n = 3$, we find

$$\mathcal{M}_3[f](x;r) = \frac{1}{r} \int_0^r p(x;t) \, dt, \quad x \in \mathbb{R}^3, \ r > 0.$$

A.3 The Radon Transform

The Radon transform for a smooth function $g : \mathbb{R}^2 \to \mathbb{R}$ with compact support is defined by

$$\mathcal{R}[g] : \mathbb{R} \times S^1 \to \mathbb{R}, \quad \mathcal{R}[g](r, \theta) = \int_{-\infty}^{\infty} g(r\theta + u\theta^{\perp}) \, du. \qquad (A.9)$$

The Radon transform can be inverted and we have the explicit formula

$$\mathcal{R}^{-1}[G](\xi) = -\frac{1}{(2\pi)^2} \int_{-\infty}^{\infty} \frac{1}{r} \int_{S^1} \partial_r G(r + \langle \theta, \xi \rangle, \theta) \, d\theta \, dr$$

for the inverse Radon transform, see e.g. [16].

A.4 Mathieu Functions

The Mathieu Functions are solutions of the Mathieu equation

$$u''(s) + (a - 2q \cos(2s))u(s) = 0. \qquad (A.10)$$

However, we are only interested in 2π-periodic solutions. It is known, see e.g. [1], that for a fixed value $q \geq 0$, there only exists a 2π-periodic solution of the equation (A.10) for a discrete set of values $a \in \mathbb{R}$. Conventionally, the values a for which an even 2π-periodic solution exists, are labeled in increasing order as $a_n(q)$ with the Mathieu cosine functions $s \mapsto \mathrm{ce}_n(s; q)$ as corresponding solutions, $n \in \mathbb{N}_0$; and the values a for which we have an odd 2π-periodic solution are (again in increasing order) called $b_n(q)$ with the Mathieu sine functions $s \mapsto \mathrm{se}_n(s, q)$ as corresponding solutions, $n \in \mathbb{N}$. The normalization of the solutions ce_n and se_n is chosen to be

$$\int_0^{2\pi} \mathrm{ce}_n(s; q)^2 \, ds = \pi \quad \text{and} \quad \int_0^{2\pi} \mathrm{se}_n(s; q)^2 \, ds = \pi.$$

Thus, since the functions are the eigenfunctions of the symmetric operator $\partial_{ss} + 2q \cos(2s)$, the functions $\frac{1}{\sqrt{\pi}} \mathrm{ce}_n(\cdot; q)$, $\frac{1}{\sqrt{\pi}} \mathrm{se}_{n+1}(\cdot; q)$, $n \in \mathbb{N}_0$, form for every $q \geq 0$ a complete orthonormal system of $L^2([0, 2\pi])$.

References

[1] M. Abramowitz and I. A. Stegun. *Handbook of mathematical functions with formulas, graphs, and mathematical tables*, volume 55 of *National Bureau of Standards Applied Mathematics Series*. For sale by the Superintendent of Documents, U.S. Government Printing Office, Washington, D.C., 1964.

[2] P. Burgholzer, C. Hofer, G. Paltauf, M. Haltmeier, and O. Scherzer. Thermoacoustic tomography with integrating area and line detectors. *Ultrasonics, Ferroelectrics and Frequency Control, IEEE Transactions on*, 52(9):1577 –1583, sept. 2005.

[3] B. T. Cox, S. R. Arridge, K. P. Köstli, and P. C. Beard. Two-dimensional quantitative photoacoustic image reconstruction of absorption distributions in scattering media by use of a simple iterative method. *Appl. Opt.*, 45(8):1866–1875, 2006.

[4] P. Elbau, O. Scherzer, and R. Schulze. Exact reconstruction formulas in photoacoustic imaging in ellipsoidal geometries. *work in progress*, 2012.

[5] L. C. Evans. *Partial differential equations*, volume 19 of *Graduate Studies in Mathematics*. American Mathematical Society, Providence, RI, 1998.

[6] D. Finch, M. Haltmeier, and Rakesh. Inversion of spherical means and the wave equation in even dimensions. *SIAM J. Appl. Math.*, 68(2):392–412, 2007.

[7] S. Gratt, K. Passler, R. Nuster, and G. Paltauf. Photoacoustic imaging with a large, cylindrical detector. In *Digital Holography and Three-Dimensional Imaging*, page JMA51. Optical Society of America, 2010.

[8] S. Gratt, K. Passler, R. Nuster, and G. Paltauf. Photoacoustic section imaging with an integrating cylindrical detector. In H. J. C. M. Sterenborg and I. A. Vitkin, editors, *Novel Biophotonic Techniques and Applications*, volume 8090, page 80900K. SPIE, 2011.

[9] S. Gratt, K. Passler, R. Nuster, and G. Paltauf. Photoacoustic section imaging with an integrating cylindrical detector. *Biomed. Opt. Express*, 2(11):2973–2981, Nov 2011.

[10] M. Haltmeier, O. Scherzer, P. Burgholzer, R. Nuster, and G. Paltauf. Thermoacoustic tomography and the circular Radon transform: exact inversion formula. *Math. Models Methods Appl. Sci.*, 17(4):635–655, 2007.

[11] K. P. Köstli and P. C. Beard. Two-dimensional photoacoustic imaging by use of fourier-transform image reconstruction and a detector with an anisotropic response. *Appl. Opt.*, 42(10):1899–1908, Apr 2003.

[12] R. A. Kruger, D. R. Reinecke, and G. A. Kruger. Thermoacoustic computed tomography – technical considerations. *Medical physics*, 26(9):1832–1837, 1999.

[13] P. Kuchment and L. Kunyansky. Mathematics of thermoacoustic tomography. *European J. Appl. Math.*, 19(2):191–224, 2008.

[14] L. A. Kunyansky. A series solution and a fast algorithm for the inversion of the spherical mean Radon transform. *Inverse Problems*, 23(6):S11–S20, 2007.

[15] R. Ma, A. Taruttis, V. Ntziachristos, and D. Razansky. Multispectral optoacoustic tomography (msot) scanner for whole-body small animal imaging. *Opt. Express*, 17(24):21414–21426, Nov 2009.

[16] F. Natterer. *The mathematics of computerized tomography*, volume 32 of *Classics in Applied Mathematics*. Society for Industrial and Applied Mathematics (SIAM), Philadelphia, PA, 2001. Reprint of the 1986 original.

[17] F. Natterer. Photo-acoustic inversion in convex domains. *preprint*, 2011.

[18] S. J. Norton. Reconstruction of a two-dimensional reflecting medium over a circular domain: exact solution. *J. Acoust. Soc. Amer.*, 67(4):1266–1273, 1980.

[19] S. J. Norton and M. Linzer. Ultrasonic reflectivity imaging in three dimensions: Exact inverse scattering solutions for plane, cylindrical, and spherical apertures. *Biomedical Engineering, IEEE Transactions on*, BME-28(2):202 –220, feb. 1981.

[20] V. P. Palamodov. A new reconstruction method in integral geometry. *arXiv:1109.2294v2*, 2011.

[21] V. P. Palamodov. A uniform reconstruction formula in integral geometry. *arXiv:1111.6514v1*, 2011.

[22] G. Paltauf, R. Nuster, and P. Burgholzer. Weight factors for limited angle photoacoustic tomography. *Physics in Medicine and Biology*, 54(11):3303, 2009.

[23] G. Paltauf, R. Nuster, M. Haltmeier, and P. Burgholzer. Photoacoustic tomography with integrating area and line detectors. In *Photoacoustic Imaging and Spectroscopy*, pages 251–263. CRC Press, 2009.

[24] D. Razansky, M. Distel, C. Vinegoni, R. Ma, N. Perrimon, R. W. Köster, and V. Ntziachristos. Multispectral opto-acoustic tomography of deep-seated fluorescent proteins in vivo. *Nature Photonics*, 3(7):412–417, 2009.

[25] M. Xu and L. V. Wang. Time-domain reconstruction for thermoacoustic tomography in a spherical geometry. *Medical Imaging, IEEE Transactions on*, 21(7):814 –822, july 2002.

[26] M. Xu and L. V. Wang. Universal back-projection algorithm for photoacoustic computed tomography. *Phys. Rev. E*, 71:016706, Jan 2005.

[27] Y. Xu, D. Feng, and L. V. Wang. Exact frequency-domain reconstruction for thermoacoustic tomography. i. planar geometry. *Medical Imaging, IEEE Transactions on*, 21(7):823 –828, july 2002.

[28] Y. Xu, M. Xu, and L. V. Wang. Exact frequency-domain reconstruction for thermoacoustic tomography. ii. cylindrical geometry. *Medical Imaging, IEEE Transactions on*, 21(7):829 –833, july 2002.